

Article

# Three-Dimensional Unsteady Mixed Convection Flow of Non-Newtonian Nanofluid with Consideration of Retardation Time Effects

Badreddine Ayadi <sup>1,2</sup>, Kaouther Ghachem <sup>3</sup>, Kamel Al-Khaled <sup>4</sup>, Sami Ullah Khan <sup>5</sup>, Karim Kriaa <sup>6,7</sup>, Chemseddine Maatki <sup>8,9</sup>, Nesrine Zahi <sup>10</sup> and Lioua Kolsi <sup>1,\*</sup>

- <sup>1</sup> Department of Mechanical Engineering, College of Engineering, University of Ha'il, Ha'il City 81451, Saudi Arabia
- <sup>2</sup> Laboratory of Applied Fluid Mechanics, Environment and Process Engineering "LR11ES57", National School of Engineers of Sfax (ENIS), University of Sfax, Soukra Road Km 3.5, Sfax 3038, Tunisia
- <sup>3</sup> Department of Industrial Engineering and Systems, College of Engineering, Princess Nourah bint Abdulrahman University, P.O. Box 84428, Riyadh 11671, Saudi Arabia
- <sup>4</sup> Department of Mathematics & Statistics, Jordan University of Science and Technology, P.O. Box 3030, Irbid 22110, Jordan
- <sup>5</sup> Department of Mathematics, Namal University, Mianwali 42250, Pakistan
- <sup>6</sup> Department of Chemical Engineering, College of Engineering, Imam Mohammad Ibn Saud Islamic University (IMSIU), Riyadh 11432, Saudi Arabia
- <sup>7</sup> Department of Chemical Engineering, National School of Engineers of Gabes, University of Gabes, Gabes 6029, Tunisia
- <sup>8</sup> Department of Mechanical Engineering, College of Engineering, Imam Mohammad Ibn Saud Islamic University (IMSIU), Riyadh 11432, Saudi Arabia
- <sup>9</sup> Laboratory of Metrology and Energy Systems, Energy Engineering Department, National Engineering School, University of Monastir, Monastir 5000, Tunisia
- <sup>10</sup> Applied College, Huraymila, Imam Mohammad Ibn Saud Islamic University (IMSIU), Riyadh 11432, Saudi Arabia
- \* Correspondence: lioua\_enim@yahoo.fr



**Citation:** Ayadi, B.; Ghachem, K.; Al-Khaled, K.; Khan, S.U.; Kriaa, K.; Maatki, C.; Zahi, N.; Kolsi, L. Three-Dimensional Unsteady Mixed Convection Flow of Non-Newtonian Nanofluid with Consideration of Retardation Time Effects. *Mathematics* **2023**, *11*, 1892. <https://doi.org/10.3390/math11081892>

Academic Editor: Arsen Palestini

Received: 8 March 2023

Revised: 12 April 2023

Accepted: 15 April 2023

Published: 17 April 2023



**Copyright:** © 2023 by the authors. Licensee MDPI, Basel, Switzerland. This article is an open access article distributed under the terms and conditions of the Creative Commons Attribution (CC BY) license (<https://creativecommons.org/licenses/by/4.0/>).

**Abstract:** The advances in nanotechnology led to the development of new kinds of engineered fluids called nanofluids. Nanofluids have several industrial and engineering applications, such as solar energy systems, heat conduction processes, nuclear systems, chemical processes, etc. The motivation of the present work is to analyze and explore the thermal and dynamic behaviors of a non-Newtonian fluid flow under time retardation effects. The flow is unsteady and caused by a bidirectional, periodically moving surface. In addition to the convective heat transfer and fluid flow, the radiation and chemical reactions have also been considered. The governing equations are established based on the modified Cattaneo–Christov heat flux formulation. It was found that the bidirectional velocities oscillate periodically, and that the magnitude of the oscillation increases with the retardation time. Higher temperatures occur when the porosity parameter is increased, and lower concentrations are encountered for higher values of the concentration relaxation parameter. The current results can be applied in thermal systems, heat transfer enhancement, chemical synthesis, solar systems, power generation, medical applications, the automotive industry, process industries, refrigeration, etc.

**Keywords:** heat transfer; bidirectional flow; porous medium; nanofluids; accelerating surface; chemical reaction; Oldroyd-B nanofluid

**MSC:** 76r05; 76r10

## 1. Introduction

Several studies on nanofluid applications have recently been presented. Leading to more compact systems and higher performances, nanofluids have become widely used

in heat transfer systems, the production and enhancement of energy resources, the extrusion process, the nuclear industry, and many other applications. When nanoparticles are suspended in a base fluid, the suspension becomes characterized by enhanced thermophysical properties. Nanoparticles are particles with dimensions in the nanometer range, typically between 1 and 100 nanometers in size. The size of nanoparticles can vary depending on their composition, shape, and method of synthesis. In general, nanoparticles smaller than 10 nanometers tend to have unique physical and chemical properties due to their high surface-area-to-volume ratio, while those larger than 100 nanometers start to exhibit bulk-like behavior. These nanoparticles are uniformly distributed in the base liquid to enhance the thermal impact of the base materials. Such predictions were first experimentally confirmed by Choi [1]. Buongiorno [2] presented a detailed description of nanofluid convective heat transfer with a focus on the thermophoretic and Brownian motion effects. Hayat et al. [3] investigated the hydrothermal behavior of a nanofluid flow under the effect of an external magnetic field. Sui et al. [4] studied the Cattaneo–Christov double diffusive convection of a Maxwell nanofluid past a stretching sheet. Hsiao [5] presented a numerical study on the micropolar nanofluid flow by considering the MHD and viscous dissipation effects. Turkyilmazoglu [6] considered free and circular jet cooling using nanofluids. Ahmed et al. [7] presented a study on the stagnation point of nanofluid flow past a rotating disk under the effect of a heat source. Turkyilmazoglu [8] used the Buongiorno model to study the nanofluid flow in an asymmetric channel. Tlili et al. [9] studied the bioconvective non-Newtonian nanofluid flow past a stretching cylinder by considering the effect of the activation energy. Abbasi et al. [10] studied the effect of using a hybrid nanofluid on the flow over a curved channel. Kiranakumar et al. [11] presented a comprehensive review of the electrical properties of graphene oxide nanoparticles. Waqas et al. [12] studied the effect of applying an exponential heat flux on the bioconvection of a non-Newtonian nanofluid past a moving surface. Chu et al. [13] used the Keller box method to study the radiative heat transfer of various kinds of hybrid nanofluids. Habib et al. [14] investigated the combined EHD, MHD, and activation energy effects on the bioconvective, time-dependent nanofluid flow caused by an extending sheet. Xia et al. [15] studied the entropy generation caused by the natural bioconversion of Eyring–Powell nanofluids. Waqas et al. [16] studied the bioconvective micropolar nanofluid flow under the impacts of a magnetic field, radiation, and the Joule effect. Liu et al. [17] performed a molecular dynamics study on the effect of using CuO nanoparticles on the phase-change process of a PCM. Mekheimer et al. [18] studied numerically the nanoparticle drug injection in blood to detect diseased organs.

The characteristics of non-Newtonian materials are very important in industrial frameworks and engineering processes. For example, non-Newtonian polymers have several applications in manufacturing processes and chemical industries. Based on their fluid behavior, non-Newtonian liquids are classified into diverse categories. The Maxwell model describes non-Newtonian viscous flow on a long timescale. However, retardation time features are novel rheological consequences that are observed in some non-Newtonian liquids. Such characteristics are identified with the help of the Oldroyd-B fluid model. Kumar et al. [19] presented a study on the rheological behavior of Oldroyd-B fluid with consideration of viscous dissipation and the Joule and radiation effects. Sajid et al. [20] numerically investigated the mixed convection of Oldroyd-B liquid under the effects of viscous dissipation and an external magnetic field. Irfan et al. [21] tested the effect of considering a variable thermal conductivity on the double diffusive convection of Oldroyd-B nanofluid. Bai et al. [22] presented a numerical study on the transient Oldroyd-B double diffusive flow. Roy and Pop [23] conducted an investigation on the mixed convection of Oldroyd-B nanofluid past a shrinking surface. Mabood et al. [24] predicted the effect of radiation and chemical reactions on the rheological behavior of Oldroyd-B nanofluid.

The main objective of the current study is to observe the thermal and hydrodynamic behaviors of Oldroyd-B nanofluid flow caused by a bidirectionally oscillating porous surface. To perform this study, the unsteady mathematical model governing the coupled

heat and mass transfer phenomena is developed using the Cattaneo–Christov thermal flux model, and HAM is used to find the semi-analytical solution. The effects of chemical reactions and radiation on the flow and heat and mass transfer are presented in terms of their velocity, temperature, and concentration profiles.

### 2. Problem Formulation

The Oldroyd-B nanofluid flow over a bidirectional, periodically oscillating porous surface is considered in the current study. The three-dimensional flow is caused by a moving surface with time-dependent velocity. The bidirectional surface is maintained at horizontal and vertical velocities expressed as  $u = u_w = ax \sin \omega t$  and  $v = v_w = by \sin \omega t$ , respectively. Here,  $\omega$  and  $b$  are the angular frequencies and stretching rate, respectively. Following the cartesian coordinates,  $x$  and  $y$  are being continued in the surface direction while the  $z$  axis is toward the normal direction. For oscillatory phenomena, it has been assumed that the magnitude of oscillation is small in such a manner that the flow regime is kept laminar [25–27]. The heat and concentration equations are established via the modified heat and mass flux theories. In addition, the chemical reaction effect is considered in the concentration equation. Based on the above-mentioned assumptions, the governing equations are expressed as follows [25–27]:

$$\frac{\partial v}{\partial y} + \frac{\partial u}{\partial x} + \frac{\partial w}{\partial z} = 0, \tag{1}$$

$$\begin{aligned} & \left( \frac{\partial u}{\partial y} \right) v + \left( \frac{\partial u}{\partial x} \right) u + \frac{\partial u}{\partial t} + \left( \frac{\partial u}{\partial z} \right) w + \lambda_1 \left( \begin{aligned} & 2 \left( w \frac{\partial^2 u}{\partial z \partial t} + v w \frac{\partial^2 u}{\partial y \partial z} \right) + 2 \left( u v \frac{\partial^2 u}{\partial x \partial y} \right) \\ & + \frac{\partial^2 u}{\partial t^2} + v^2 \frac{\partial^2 u}{\partial y^2} + u^2 \frac{\partial^2 u}{\partial x^2} + w^2 \frac{\partial^2 u}{\partial z^2} \\ & + 2 \left( v \frac{\partial^2 u}{\partial y \partial t} \right) + 2 \left( u w \frac{\partial^2 u}{\partial x \partial z} + u \frac{\partial^2 u}{\partial x \partial t} \right) \end{aligned} \right) - v \frac{\partial^2 u}{\partial z^2} \\ & + v \lambda_2 \left( \frac{\partial^2 v}{\partial z^2} \frac{\partial u}{\partial y} + \frac{\partial^2 w}{\partial z^2} \frac{\partial u}{\partial z} + \frac{\partial^2 u}{\partial z^2} \frac{\partial u}{\partial x} \right) \\ & = v \lambda_2 \left( \frac{\partial^3 u}{\partial z^2 \partial t} + v \frac{\partial^3 u}{\partial y \partial z^2} + u \frac{\partial^3 u}{\partial x \partial z^2} + w \frac{\partial^3 u}{\partial z^3} \right) - \frac{v u}{k_p}, \end{aligned} \tag{2}$$

$$\begin{aligned} & u \left( \frac{\partial v}{\partial x} \right) + v \left( \frac{\partial v}{\partial y} \right) + w \left( \frac{\partial v}{\partial z} \right) + \frac{\partial v}{\partial t} + \lambda_1 \left( \begin{aligned} & 2 \left( w \frac{\partial^2 v}{\partial z \partial t} \right) + 2 \left( u v \frac{\partial^2 v}{\partial x \partial y} + v w \frac{\partial^2 v}{\partial y \partial z} \right) \\ & + \frac{\partial^2 v}{\partial t^2} + v^2 \frac{\partial^2 v}{\partial y^2} + w^2 \frac{\partial^2 v}{\partial z^2} + u^2 \frac{\partial^2 v}{\partial x^2} \\ & + 2 \left( v \frac{\partial^2 v}{\partial y \partial t} \right) + 2 \left( u w \frac{\partial^2 v}{\partial x \partial z} + u \frac{\partial^2 v}{\partial x \partial t} \right) \end{aligned} \right) - v \frac{\partial^2 v}{\partial z^2} \\ & + v \lambda_2 \left( \frac{\partial v}{\partial y} \frac{\partial^2 v}{\partial z^2} + \frac{\partial^2 w}{\partial z^2} \frac{\partial v}{\partial z} + \frac{\partial v}{\partial x} \frac{\partial^2 u}{\partial z^2} \right) = v \lambda_2 \left( \frac{\partial^3 v}{\partial z^2 \partial t} + w \frac{\partial^3 v}{\partial z^3} + v \frac{\partial^3 v}{\partial y \partial z^2} + u \frac{\partial^3 v}{\partial x \partial z^2} \right) - \frac{v u}{k_p}, \end{aligned} \tag{3}$$

$$\begin{aligned} & u \frac{\partial T}{\partial x} + v \frac{\partial T}{\partial y} + w \frac{\partial T}{\partial z} + \frac{\partial T}{\partial t} + \delta_2 \left[ \begin{aligned} & 2u \frac{\partial^2 T}{\partial x \partial t} + w^2 \frac{\partial^2 T}{\partial z^2} + v^2 \frac{\partial^2 T}{\partial y^2} + u^2 \frac{\partial^2 T}{\partial x^2} + 2w \frac{\partial^2 T}{\partial z \partial t} + w \frac{\partial u}{\partial z} \frac{\partial T}{\partial x} \\ & + v \left( \frac{\partial T}{\partial z} \frac{\partial w}{\partial y} + \frac{\partial T}{\partial y} \frac{\partial v}{\partial y} \right) + \frac{\partial w}{\partial t} \frac{\partial T}{\partial z} + u \left( \frac{\partial T}{\partial y} \frac{\partial v}{\partial x} + \frac{\partial T}{\partial x} \frac{\partial u}{\partial x} + \frac{\partial T}{\partial z} \frac{\partial w}{\partial x} \right) \\ & + \frac{\partial u}{\partial t} \frac{\partial T}{\partial x} + \frac{\partial v}{\partial t} \frac{\partial T}{\partial y} + \frac{\partial^2 T}{\partial t^2} + v \frac{\partial u}{\partial y} \frac{\partial T}{\partial x} + w \frac{\partial v}{\partial z} \frac{\partial T}{\partial y} \\ & + 2v \left( u \frac{\partial^2 T}{\partial x \partial y} + w \frac{\partial^2 T}{\partial y \partial z} + \frac{\partial^2 T}{\partial y \partial t} \right) + w \left( 2u \frac{\partial^2 T}{\partial x \partial z} + \frac{\partial w}{\partial z} \frac{\partial T}{\partial z} \right) \end{aligned} \right] \\ & = \left( \alpha_m + \frac{16\sigma_s T_\infty^3}{3k^*(\rho c)_f} \right) \frac{\partial^2 T}{\partial z^2} + \sigma_* \left[ \frac{D_T}{T_\infty} \left( \frac{\partial T}{\partial z} \right)^2 + D_B \frac{\partial C}{\partial z} \frac{\partial T}{\partial z} \right], \end{aligned} \tag{4}$$

$$\left( \frac{\partial C}{\partial y} \right) v + \left( \frac{\partial C}{\partial x} \right) u + \frac{\partial C}{\partial t} + \left( \frac{\partial C}{\partial z} \right) w + \delta_2 \left[ \begin{aligned} &2u \frac{\partial^2 C}{\partial x \partial t} + w^2 \frac{\partial^2 C}{\partial z^2} + v^2 \frac{\partial^2 C}{\partial y^2} + u^2 \frac{\partial^2 C}{\partial x^2} \\ &+ 2w \frac{\partial^2 C}{\partial z \partial t} + w \frac{\partial u}{\partial z} \frac{\partial C}{\partial x} + v \frac{\partial v}{\partial y} \frac{\partial C}{\partial y} \\ &+ v \frac{\partial w}{\partial y} \frac{\partial C}{\partial z} + \frac{\partial v}{\partial t} \frac{\partial C}{\partial y} \\ &+ u \left( \frac{\partial C}{\partial y} \frac{\partial v}{\partial x} + \frac{\partial u}{\partial x} \frac{\partial C}{\partial x} + \frac{\partial C}{\partial z} \frac{\partial w}{\partial x} \right) \\ &+ \frac{\partial u}{\partial t} \frac{\partial C}{\partial x} + \frac{\partial^2 C}{\partial t^2} + v \frac{\partial u}{\partial y} \frac{\partial C}{\partial x} \\ &+ \frac{\partial w}{\partial t} \frac{\partial C}{\partial z} + w \frac{\partial v}{\partial z} \frac{\partial C}{\partial y} \\ &+ 2v \left( u \frac{\partial^2 C}{\partial x \partial y} + w \frac{\partial^2 C}{\partial y \partial z} + \frac{\partial^2 C}{\partial y \partial t} \right) \\ &+ w \left( 2u \frac{\partial^2 C}{\partial x \partial z} + \frac{\partial w}{\partial z} \frac{\partial C}{\partial z} \right) \end{aligned} \right] \tag{5}$$

$$= \left( \frac{D_T}{T_\infty} \right) \frac{\partial^2 T}{\partial z^2} + D_B \frac{\partial^2 C}{\partial z^2} - k_*(C - C_\infty).$$

The boundary conditions are [25–27]:

$$u = u_w = ax \sin \omega t, \quad w = 0, \quad C = C_w, \quad v = v_w = by \sin \omega t, \quad T = T_w, \quad z = 0, \tag{6}$$

$$u \rightarrow 0, \quad C \rightarrow C_\infty, \quad T \rightarrow T_\infty, \quad v \rightarrow 0, \quad \text{as } z \rightarrow \infty. \tag{7}$$

The used dimensionless variables are [25,27]:

$$\left. \begin{aligned} v &= ya g_\zeta(\zeta, \tau), \quad w = -\sqrt{va}(+g(\zeta, \tau) + f(\zeta, \tau)), \quad u = xa f_\zeta(\zeta, \tau) \\ \zeta &= \sqrt{\frac{a}{v}}z, \quad \tau = t\omega, \quad \theta(\zeta, \tau) = \frac{T - T_\infty}{T_w - T_\infty}, \quad \phi(\zeta, \tau) = \frac{C - C_\infty}{C_w - C_\infty}. \end{aligned} \right\} \tag{8}$$

Using these new variables, the governing equations become:

$$f_{\zeta\zeta\zeta} + ff_{\zeta\zeta} + gf_{\zeta\zeta} - (f_\zeta^2 + Sf_{\zeta\tau}) - Haf_\zeta - \beta_1 \left[ \begin{aligned} &S^2 f_{\zeta\tau\tau} + 2Sf_\zeta f_{\zeta\tau} + (f + g)^2 f_{\zeta\zeta\zeta} \\ &- 2(f + g)(Sf_{\zeta\zeta\tau} + f_\zeta f_{\zeta\zeta}) \end{aligned} \right] + \beta_2 \left[ \begin{aligned} &Sf_{\zeta\zeta\zeta\tau} + f_{\zeta\zeta}(g_{\zeta\zeta} + f_{\zeta\zeta}) \\ &-(f + g)f_{\zeta\zeta\zeta\zeta} \end{aligned} \right], \tag{9}$$

$$g_{\zeta\zeta\zeta} + (g + f)g_{\zeta\zeta} - Haf_\zeta - (g_\zeta^2 + Sg_{\zeta\tau}) + \beta_2 \left[ \begin{aligned} &g_{\zeta\zeta}(f_{\zeta\zeta} + g_{\zeta\zeta}) \\ &+ Sg_{\zeta\zeta\zeta\tau} - (g + f)g_{\zeta\zeta\zeta\zeta} \end{aligned} \right] - \beta_1 \left[ \begin{aligned} &S^2 g_{\zeta\tau\tau} + g_{\zeta\zeta\zeta}(f + g)^2 + 2Sg_\zeta g_{\zeta\tau} \\ &- 2(Sg_{\zeta\zeta\tau} + g_{\zeta\zeta}g_{\zeta\zeta})(f + g) \end{aligned} \right] = 0, \tag{10}$$

$$\frac{(1 + Rd)}{Pr} \theta_{\zeta\zeta} + (Nb\theta_\zeta \phi_\zeta - S\theta_\tau + Nt\theta_\zeta^2 + (g + f)\theta_\zeta) - \delta_T \left( \begin{aligned} &S^2 \theta_{\tau\tau} - S(f_\tau \theta_\zeta + g_\tau \theta_\zeta) \\ &- 2S(g + f)\theta_{\tau\zeta} + (g + f)^2 \theta_{\zeta\zeta} \\ &+ (f_\zeta + g_\zeta)(f + g)\theta_\zeta \end{aligned} \right) = 0, \tag{11}$$

$$\phi_{\zeta\zeta} + LePr[(g + f)\phi_\zeta - S\phi_\tau - Kr\phi] + \frac{Nt}{Nb} \theta_{\zeta\zeta} - Sc\delta_c \left( \begin{aligned} &S^2 \phi_{\tau\tau} - S(f_\tau \phi_\zeta + g_\tau \phi_\zeta) \\ &- 2S(g + f)\phi_{\tau\zeta} + (g + f)^2 \phi_{\zeta\zeta} \\ &+ (f_\zeta + g_\zeta)(f + g)\phi_\zeta \end{aligned} \right) = 0. \tag{12}$$

The dimensionless boundary conditions are as follows:

$$\left. \begin{aligned} g(0, \tau) = 0, f(0, \tau) = 0, f_{\xi}(0, \tau) = \sin \tau, g_{\xi}(0, \tau) = \gamma \sin \tau, \theta(0, \tau) = 1 \\ \phi(0, \tau) = 1, g_{\xi}(\infty, \tau) = 0, f_{\xi}(\infty, \tau) = 0, \theta(\infty, \tau) = 0, \phi(\infty, \tau) = 0. \end{aligned} \right\} \quad (13)$$

The dimensionless parameters  $\beta_1, \beta_2$  (Deborah numbers),  $Nb$  (Brownian motion),  $Le$  (Lewis number),  $Kr$  (chemical reaction),  $\gamma$  (stretching ratio constant),  $Kr$  (reaction constant),  $\delta_T$  (thermal relaxation constant),  $\delta_c$  (concentration relaxation constant),  $S$  (ratio of frequency to stretching rate),  $Pr$  (Prandtl number), and  $Nt$  (thermophoresis) are defined as:

$$\left. \begin{aligned} Le = \frac{\alpha_m}{D_B}, Kr = \frac{k_*}{a}, \beta_1 = \lambda_1 a, \beta_2 = \lambda_2 a, Pr = \frac{\nu}{\alpha_m}, S = \frac{\omega}{a}, Nb = \frac{\sigma_* D_B (C_w - C_{\infty})}{\nu} \\ R = \frac{16\sigma_s T_{\infty}^3}{3kk^*}, \delta_c = \delta_2 a, \gamma = \frac{b}{a}, Nt = \frac{\sigma_* D_T (T_w - T_{\infty})}{\nu T_{\infty}}, Ha = \frac{\nu}{ak_p}, \delta_T = \delta_1 a. \end{aligned} \right\} \quad (14)$$

The local Sherwood and Nusselt numbers are expressed by the following relations [27]:

$$(Re_x)^{-1/2} Nu_x = -(1 + R)\theta_{\xi}(0, \tau), Sh_x (Re_x)^{-1/2} = -\phi_{\xi}(0, \tau). \quad (15)$$

where  $Re_x$  is the local Reynolds number.

### 3. Homotopy Analytical Method

The resolutions of the formulated model are performed analytically with the implementation of the homotopy analysis scheme. The motivations for using the homotopy analysis method are justified, as this scheme provides high accuracy and little error. It should also be mentioned that the HAM method does not have any limitations related to the fixation of any small or large parameters [28–30]. The initial guesses for performing simulations are:

$$\left. \begin{aligned} f_0(\xi, \tau) = (1 - e^{-\xi}) \sin \tau, g_0(\xi, \tau) = \gamma(1 - e^{-\xi}) \sin \tau, \\ \theta_0(\xi, \tau) = e^{-\xi}, \phi_0(\xi, \tau) = e^{-\xi}. \end{aligned} \right\} \quad (16)$$

The use of the linear operators ( $\Upsilon$ ):

$$\Upsilon_f = \frac{\partial^3}{\partial \xi^3} - \frac{\partial}{\partial \xi}, \quad \Upsilon_g = \frac{\partial^3}{\partial \xi^3} - \frac{\partial}{\partial \xi}, \quad \Upsilon_{\theta} = \frac{\partial^2}{\partial \xi^2} - 1, \quad \Upsilon_{\phi} = \frac{\partial^2}{\partial \xi^2} - 1. \quad (17)$$

gives the following equations:

$$\left. \begin{aligned} l_f [\kappa_1 + \kappa_2 e^{\xi} + \kappa_3 e^{-\xi}] = 0, \quad l_g [\kappa_4 + \kappa_5 e^{\xi} + \kappa_6 e^{-\xi}] = 0, \\ l_{\theta} [\kappa_7 e^{\xi} + \kappa_8 e^{-\xi}] = 0, \quad l_{\phi} [\kappa_9 e^{\xi} + \kappa_{10} e^{-\xi}] = 0. \end{aligned} \right\} \quad (18)$$

### 4. Convergence of HAM

The convergence regime is estimated with the proper values of auxiliary factors  $h_f, h_{\theta}, h_g$  and  $h_{\phi}$ . The feasible region for ensuring the solution validity is highlighted with plotted  $h$ -curves. Figure 1 is presented to predict this convergence region. The convergence regime is defined by  $-1.4 \leq h_f \leq 0.2, -1.4 \leq h_{\theta} \leq -0.2, -1.3 \leq h_g \leq -0.1$  and  $-1.3 \leq h_{\phi} \leq -0.35$ .

This section is dedicated to exploring the effects of the governing parameters on the flow, temperature, and concentration fields. The formulated mathematical problem is associated with the theoretical flow assumptions instead of any experimental data. Therefore, physical analysis is performed for ranges of governing parameters as follows:  $0 \leq Ha \leq 0.3, 0 \leq \beta_2 \leq 1.4, 0.1 \leq \delta_T \leq 1.2, 0.1 \leq Pr \leq 1.2, 0.1 \leq Nb \leq 1.2, 0.1 \leq Rd \leq 1.2$ , and  $0.2 \leq \delta_c \leq 0.8, 0.0 \leq Kr \leq 0.5$ . Figure 2a,b illustrate the velocity component profiles  $f_{\xi}$  and  $g_{\xi}$  for various values of the porosity parameter  $Ha$ . A declining behavior in both

velocity components is observed when  $Ha$  is increased. Physically, this reduction is due to the reduced permeability of the porous media. Figure 3a,b present the effects of the retardation time factor  $\beta_2$  on  $f_\xi$  and  $g_\xi$ . Both velocity components have larger values for higher values of  $\beta_2$ . This increase is due to the intensification of the flow caused by the retardation time. In fact, the retardation time is associated with the rest position attained by fluid particles. Figure 4a,b show the effect of the retardation parameter  $\beta_2$  on  $f_\xi$  and  $g_\xi$ . The increase in  $\beta_2$ , leads to an increase in velocity. In both graphs, a phase shift of smaller magnitude is noticed.

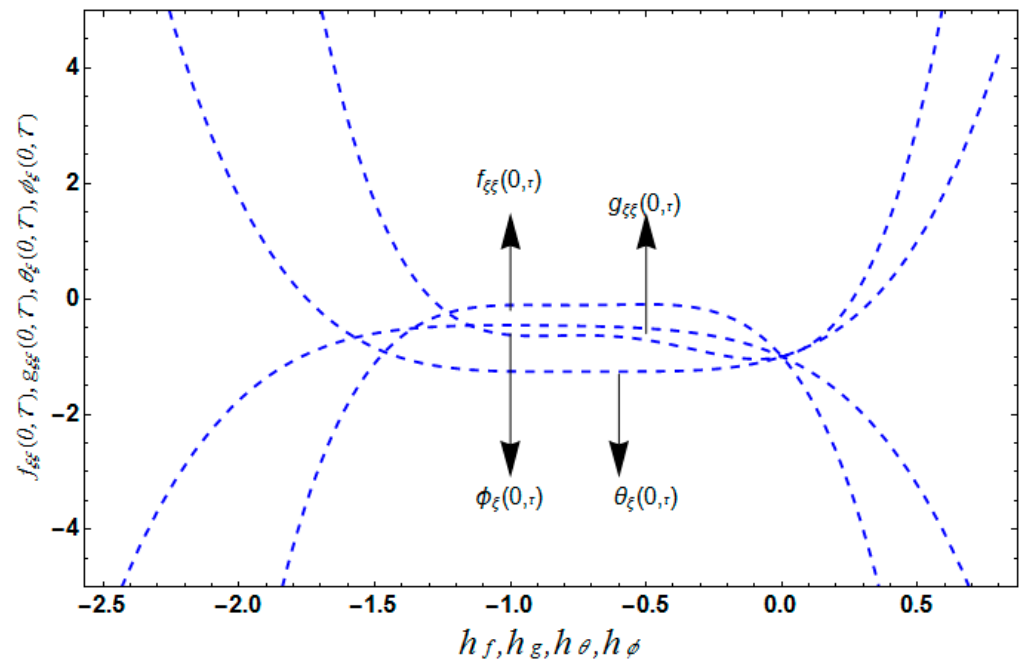


Figure 1.  $h$ -curves for all profiles.

(a)

(b)

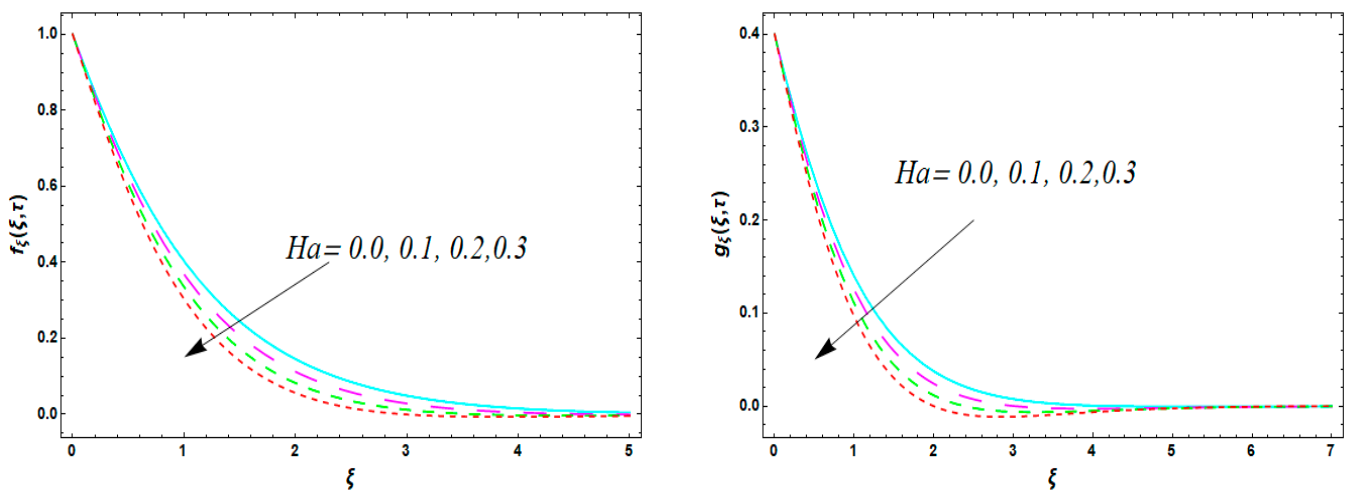


Figure 2. (a) Profiles of  $f_\xi$  for various  $Ha$  values; (b) profiles of  $g_\xi$  for various  $Ha$  values.

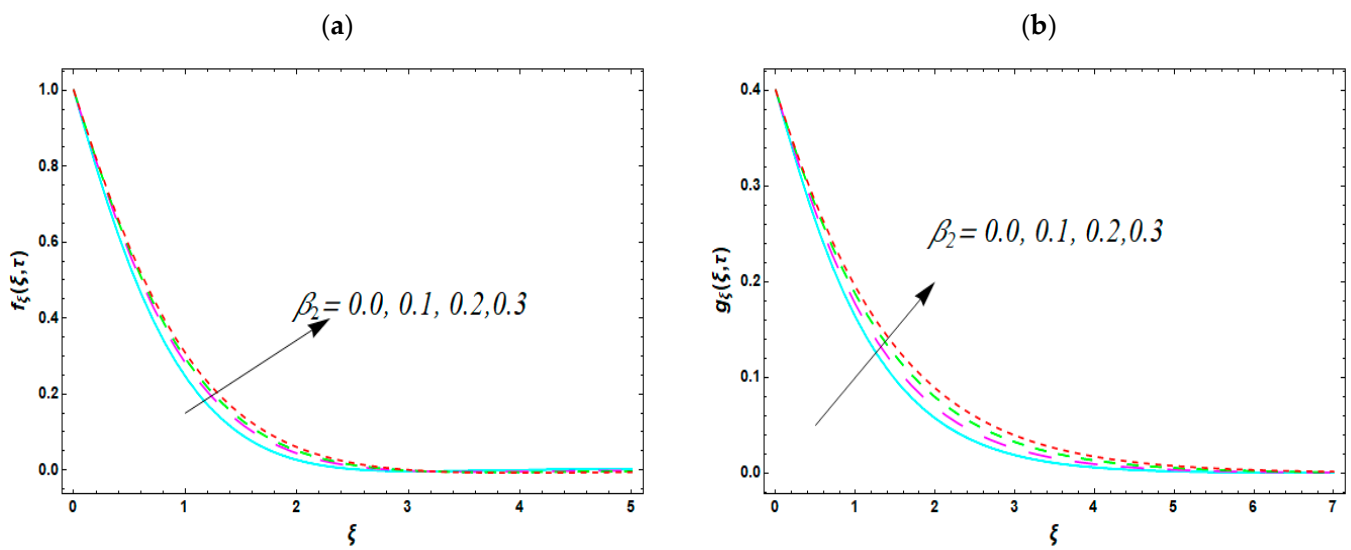


Figure 3. (a) Profiles of  $f_\xi$  for various  $\beta_2$  values; (b) profiles of  $g_\xi$  for various  $\beta_2$  values.

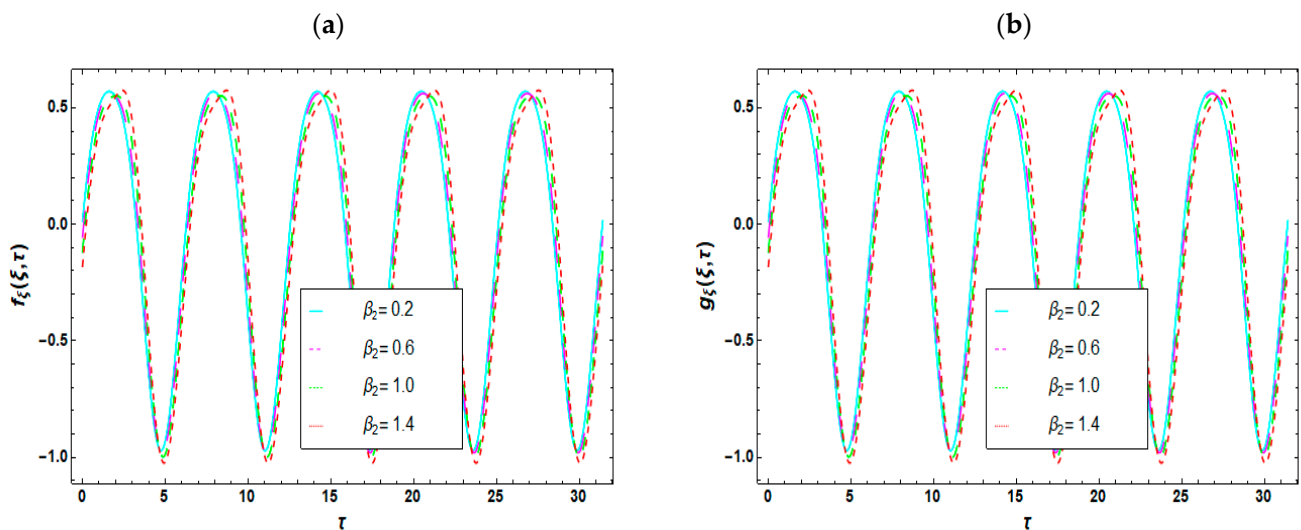


Figure 4. (a) Temporal variations in  $f_\xi$  for various  $\beta_2$  values and (b) temporal variations in  $g_\xi$  for various  $\beta_2$  values.

The results illustrated in Figure 5a report the effects of  $\delta_T$  on the behavior of the temperature profile  $\theta$ . Lower temperatures are encountered when the thermal relaxation factor  $\delta_T$  is increased. This decrease leads to a lower heat transfer rate. Figure 5b illustrates the temperature profile  $\theta$  for various Prandtl number  $Pr$  values. The Prandtl number is inversely proportional to the thermal diffusivity. Thus, the increase in  $Pr$  values, leads to a reduction in temperature. In Figure 5c, the effect of increasing the Brownian motion constant  $N_b$  on the temperature field is presented. Higher temperatures occur for larger values of  $N_b$ . Physically, Brownian motion is based on the random movement of heated particles, some of which collide with each other. This collision enhances thermal transport. The effect of the radiation parameter  $Rd$  on the temperature  $\theta$  profile is exposed in Figure 5d. The increase in  $Rd$  leads to higher temperature values. This is due to the enhancement of heat transfer by the combined effects of convective and radiative heat transfers. Figure 6a–e illustrate the changes in concentration profile  $\phi$  caused by the variation in the porosity parameter  $Ha$ , the Lewis number  $Le$ , the concentration relaxation parameter  $\delta_C$ , the reaction parameter  $Kr$ , and the Brownian parameter  $Nb$ . As presented in Figure 6a, due to the change in the porosity parameter, an increase in the concentration is exhibited. Physically,

such observations are due to the permeability of the porous space. From Figure 6b, it is concluded that the increase in  $Le$  reduces the concentration value  $\phi$ . The results presented in Figure 6c–e demonstrate that the increases in  $\delta_C$ ,  $Kr$ , and  $Nb$  lead to lower values of concentration. Table 1 presents the effect of the governing parameters on the Nusselt number. It is noticed that the increase in  $Pr$  leads to an enhancement of the heat transfer rate, while the opposite occurs for  $Nb$  and  $Nt$ . Similarly, Table 2 shows the effects of the governing parameters on the Sherwood number. An important enhancement of the mass transfer is noticed for higher values of  $Le$  and  $N_b$ .

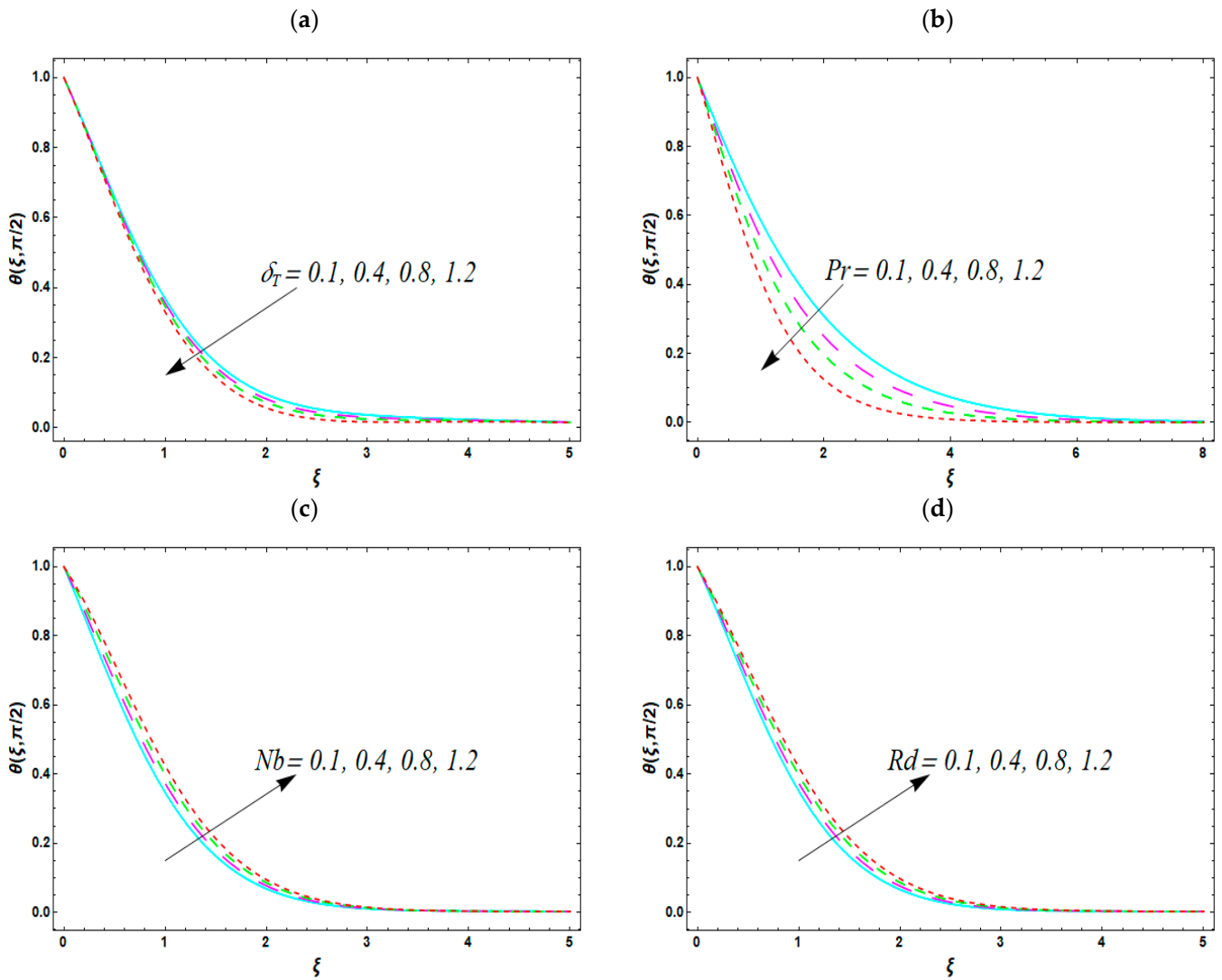


Figure 5. Temperature profiles for various values of (a)  $\delta_T$ , (b)  $Pr$ , (c)  $N_b$  and (d)  $Rd$ .

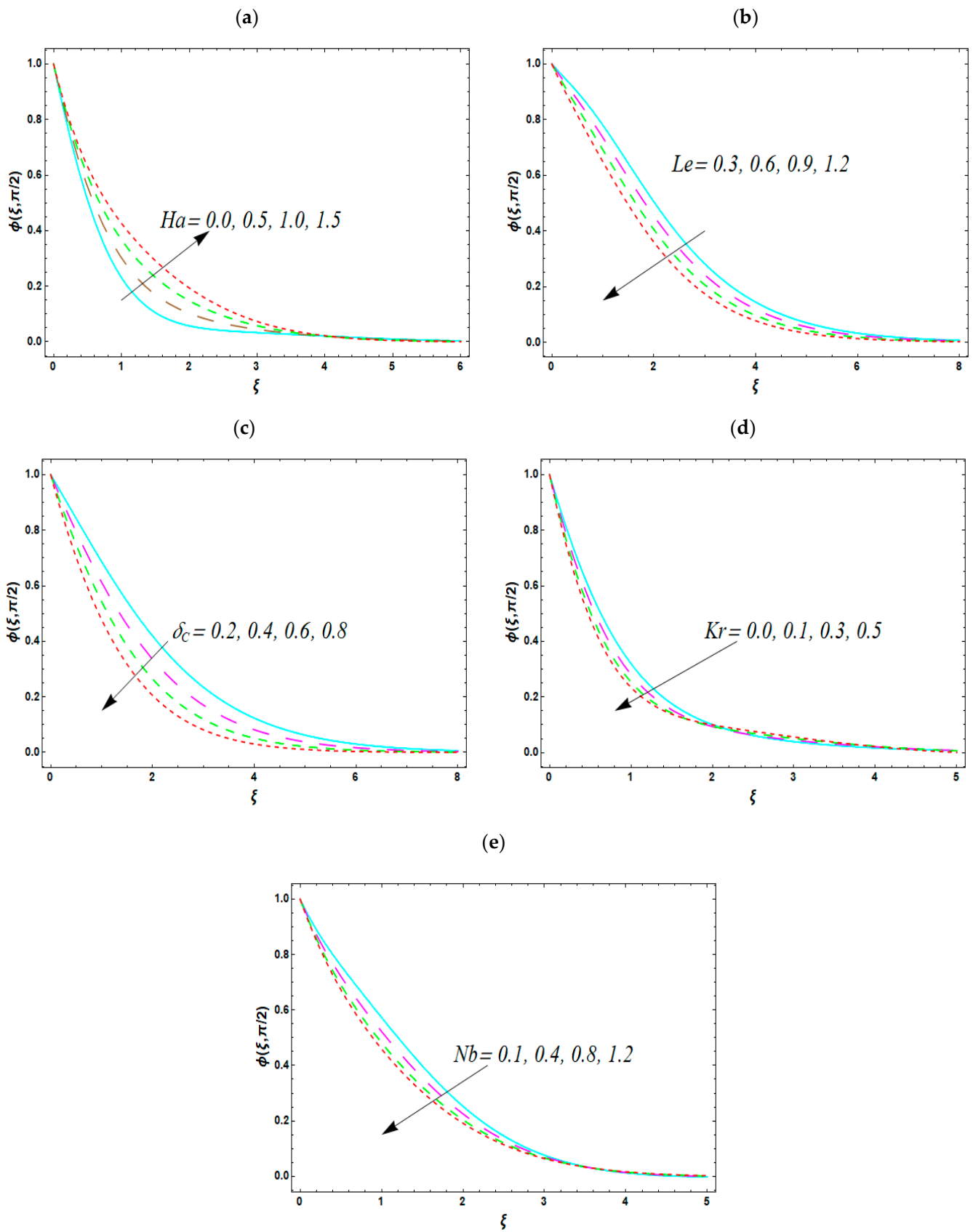


Figure 6. Concentration profiles for various values of (a)  $Ha$ , (b)  $Le$ , (c)  $\delta_C$ , (d)  $Kr$  and (e)  $Nb$ .

**Table 1.** Evaluation of Nusselt number at various governing parameters.

| Pr  | Le  | $N_b$ | $N_t$ | $\frac{Nu_x}{(Re_x)^{1/2}}$ |
|-----|-----|-------|-------|-----------------------------|
| 0.2 | 0.1 | 0.3   | 0.3   | 0.51425                     |
|     |     |       |       | 0.4                         |
|     |     |       |       | 0.8                         |
| 0.3 | 0.4 |       |       | 0.62317                     |
|     | 0.6 |       |       | 0.64209                     |
|     | 0.8 |       |       | 0.66324                     |
|     |     | 0.2   |       | 0.48359                     |
|     |     | 0.4   |       | 0.4556                      |
|     |     | 0.6   |       | 0.427857                    |
|     |     |       | 0.2   | 0.48053                     |
|     |     |       | 0.6   | 0.46475                     |
|     |     |       | 0.8   | 0.428857                    |

**Table 2.** Evaluation of Sherwood number at various governing parameters.

| Le  | $N_b$ | $N_t$ | $\frac{Sh_x}{(Re_x)^{1/2}}$ |
|-----|-------|-------|-----------------------------|
| 0.2 | 0.3   |       | 0.754231                    |
| 0.6 |       |       | 0.83544                     |
| 0.8 |       |       | 0.93567                     |
| 0.3 | 0.2   |       | 0.64567                     |
|     | 0.6   |       | 0.72675                     |
|     | 0.8   |       | 0.74534                     |
|     |       | 0.2   | 0.63556                     |
|     |       | 0.4   | 0.58324                     |
|     |       | 0.6   | 0.53677                     |

### 5. Conclusions

The heat and mass transfer characteristics of Oldroyd-B nanofluid are analyzed in consideration of chemical reactions and thermal radiation effects. The flow is generated by the bidirectional periodic oscillating surface. The HAM computations are performed for solution assessment. The main findings can be summarized as follows:

- ❖ A reduction in the flow intensity due to the increase in the porosity parameter is noticed.
- ❖ No phase shift of the oscillating velocity is encountered for all the considered parameters.
- ❖ An augmentation of the velocity magnitude occurs when the oscillation frequency ratio is increased.
- ❖ The retardation parameter causes an increase in velocity.
- ❖ The increase in the thermal relaxation factor causes a reduction in temperature.
- ❖ The porosity parameters enhance the thermal and concentration profiles.
- ❖ An augmentation of the heat transfer occurs when the radiative parameter is increasing.
- ❖ Lower concentrations are encountered for higher values of the Prandtl and Lewis numbers.
- ❖ The local Nusselt number increases with the Lewis and Prandtl numbers.
- ❖ The current analysis can be extended by modifying the model, evaluating the entropy generation, performing a sensitivity analysis, considering hybrid nanofluids, using an artificial neural network, etc.

**Author Contributions:** Conceptualization, B.A., K.G. and L.K.; Methodology, K.A.-K., S.U.K., K.K. and L.K.; Software, B.A., K.G. and N.Z.; Formal analysis, K.G., S.U.K., C.M. and L.K.; Investigation, B.A., K.G. and S.U.K.; Writing—original draft, B.A., K.G., K.A.-K., S.U.K., K.K., C.M., N.Z. and L.K.; Writing—review & editing, B.A., K.G., K.A.-K., S.U.K., K.K., C.M., N.Z. and L.K.; Project administration, K.G.; Funding acquisition, K.G. All authors have read and agreed to the published version of the manuscript.

**Funding:** Princess Nourah bint Abdulrahman University Researchers Supporting Project number (PNURSP2023R41), Princess Nourah bint Abdulrahman University, Riyadh, Saudi Arabia.

**Data Availability Statement:** Not available.

**Conflicts of Interest:** The authors declare no conflict of interest.

## Nomenclature

|             |                                       |
|-------------|---------------------------------------|
| $(u, v, w)$ | velocity components                   |
| $\omega$    | frequency                             |
| $t$         | time                                  |
| $\lambda_1$ | relaxation time                       |
| $\lambda_2$ | retardation time                      |
| $D_B$       | Brownian diffusion                    |
| $\nu$       | kinematic viscosity                   |
| $K_r$       | chemical reaction rate                |
| $D_T$       | thermal expansion coefficient         |
| $\alpha_m$  | thermal diffusivity                   |
| $\delta_1$  | thermal relaxation coefficient        |
| $\delta_2$  | concentration relaxation coefficient  |
| $\sigma_s$  | Stefan–Boltzmann constant             |
| $k^*$       | mean absorption coefficient           |
| $\beta_2$   | retardation time                      |
| $Nb$        | Brownian motion                       |
| $Le$        | Lewis number                          |
| $Kr$        | chemical reaction                     |
| $\gamma$    | stretching ratio constant             |
| $Kr$        | reaction constant                     |
| $\delta_T$  | thermal relaxation constant           |
| $\delta_c$  | concentration relaxation constant     |
| $S$         | ratio of frequency to stretching rate |
| $Pr$        | Prandtl number                        |
| $Nt$        | thermophoresis                        |

## References

- Choi, S.U.S. *Enhancing Thermal Conductivity of Fluids with Nanoparticles*. 231; American Society of Mechanical Engineers: New York, NY, USA, 1995; pp. 99–106.
- Buongiorno, J. Convective Transport in Nanofluids. *J. Heat Transfer*. **2006**, *128*, 240–250. [[CrossRef](#)]
- Hayat, T.; Kiyani, M.; Ahmad, I.; Ahmad, B. On analysis of magneto Maxwell nano-material by surface with variable thickness. *Int. J. Mech. Sci.* **2017**, *131–132*, 1016–1025. [[CrossRef](#)]
- Sui, J.; Zheng, L.; Zhang, X. Boundary layer heat and mass transfer with Cattaneo–Christov double-diffusion in upper-convected Maxwell nanofluid past a stretching sheet with slip velocity. *Int. J. Therm. Sci.* **2016**, *104*, 461–468. [[CrossRef](#)]
- Hsiao, K.-L. Micropolar nanofluid flow with MHD and viscous dissipation effects towards a stretching sheet with multimedia feature. *Int. J. Heat Mass Transf.* **2017**, *112*, 983–990. [[CrossRef](#)]
- Turkyilmazoglu, M. Free and circular jets cooled by single phase nanofluids. *Eur. J. Mech.—B/Fluids* **2019**, *76*, 1–6. [[CrossRef](#)]
- Ahmed, J.; Khan, M.; Ahmad, L. Stagnation point flow of Maxwell nanofluid over a permeable rotating disk with heat source/sink. *J. Mol. Liq.* **2019**, *287*, 110853. [[CrossRef](#)]
- Turkyilmazoglu, M. Buongiorno model in a nanofluid filled asymmetric channel fulfilling zero net particle flux at the walls. *Int. J. Heat Mass Transf.* **2018**, *126*, 974–979. [[CrossRef](#)]
- Tlili, I.; Waqas, H.; Almaneea, A.; Khan, S.U.; Imran, M. Activation Energy and Second Order Slip in Bioconvection of Oldroyd-B Nanofluid over a Stretching Cylinder: A Proposed Mathematical Model. *Processes* **2019**, *7*, 914. [[CrossRef](#)]

10. Abbasi, A.; Farooq, W.; Tag-ElDin, E.S.M.; Khan, S.U.; Khan, M.I.; Guedri, K.; Elattar, S.; Waqas, M.; Galal, A.M. Heat Transport Exploration for Hybrid Nanoparticle (Cu, Fe<sub>3</sub>O<sub>4</sub>)—Based Blood Flow via Tapered Complex Wavy Curved Channel with Slip Features. *Micromachines* **2022**, *13*, 1415. [[CrossRef](#)]
11. Kiranakumar, H.V.; Thejas, R.; Naveen, C.S.; Mijaz Khan Prasanna, G.D.; Reddy, S.; Oreijah, M.; Guedri, K.; Bafakeeh, O.T.; Jameel, M. A review on electrical and gas-sensing properties of reduced graphene oxide-metal oxide nanocomposites. *Biomass Convers. Biorefin.* **2022**, 1–11. [[CrossRef](#)]
12. Waqas, H.; Oreijah, M.; Guedri, K.; Khan, S.U.; Yang, S.; Yasmin, S.; Khan, M.I.; Bafakeeh, O.T.; Tag-ElDin, E.S.M.; Galal, A.M. Gyrotactic Motile Microorganisms Impact on Pseudoplastic Nanofluid Flow over a Moving Riga Surface with Exponential Heat Flux. *Crystals* **2022**, *12*, 1308. [[CrossRef](#)]
13. Chu, Y.-M.; Khan, M.I.; Abbas, T.; Sidi, M.O.; Alharbi, K.A.M.; Alqsair, U.F.; Khan, S.U.; Malik, M. Radiative thermal analysis for four types of hybrid nanoparticles subject to non-uniform heat source: Keller box numerical approach. *Case Stud. Therm. Eng.* **2022**, *40*, 102474. [[CrossRef](#)]
14. Habib, D.; Salamat, N.; Abdal, S.; Siddique, I.; Ang, M.C.; Ahmadian, A. On the role of bioconvection and activation energy for time dependent nanofluid slip transpiration due to extending domain in the presence of electric and magnetic fields. *Ain Shams Eng. J.* **2021**, *13*, 101519. [[CrossRef](#)]
15. Xia, W.-F.; Haq, F.; Saleem, M.; Khan, M.I.; Khan, S.U.; Chu, Y.-M. Irreversibility analysis in natural bio-convective flow of Eyring-Powell nanofluid subject to activation energy and gyrotactic microorganisms. *Ain Shams Eng. J.* **2021**, *12*, 4063–4074. [[CrossRef](#)]
16. Waqas, M.; Sadiq, M.A.; Bahaidarah, H.M. Gyrotactic bioconvection stratified flow of magnetized micropolar nanoliquid configured by stretchable radiating surface with Joule heating and viscous dissipation. *Int. Commun. Heat Mass Transf.* **2022**, *138*, 106229. [[CrossRef](#)]
17. Liu, X.; Adibi, M.; Shahgholi, M.; Tlili, I.; Sajadi, S.M.; Abdollahi, A.; Li, Z.; Karimipour, A. Phase change process in a porous Carbon-Paraffin matrix with different volume fractions of copper oxide Nanoparticles: A molecular dynamics study. *J. Mol. Liq.* **2022**, *366*, 120296. [[CrossRef](#)]
18. Mekheimer, K.S.; Abo-Elkhair, R.E.; Abdelsalam, S.I.; Ali, K.K.; Moawad, A.M.A. Biomedical simulations of nanoparticles drug delivery to blood hemodynamics in diseased organs: Synovitis problem. *Int. Commun. Heat Mass Transfer* **2022**, *130*, 105756. [[CrossRef](#)]
19. Kumar, K.G.; Ramesh, G.; Giressha, B.; Gorla, R. Characteristics of Joule heating and viscous dissipation on three-dimensional flow of Oldroyd B nanofluid with thermal radiation. *Alex. Eng. J.* **2018**, *57*, 2139–2149. [[CrossRef](#)]
20. Sajid, M.; Ahmed, B.; Abbas, Z. Steady mixed convection stagnation point flow of MHD Oldroyd-B fluid over a stretching sheet. *J. Egypt. Math. Soc.* **2015**, *23*, 440–444. [[CrossRef](#)]
21. Irfan, M.; Khan, M.; Khan, W.A.; Sajid, M. Thermal and solutal stratifications in flow of Oldroyd-B nanofluid with variable conductivity. *Appl. Phys. A* **2018**, *124*, 674. [[CrossRef](#)]
22. Bai, Y.; Tang, Q.; Zhang, Y. Unsteady MHD oblique stagnation slip flow of Oldroyd-B nanofluids by coupling Cattaneo-Christov double diffusion and Buongiorno model. *Chin. J. Phys.* **2022**, *79*, 451–470. [[CrossRef](#)]
23. Roy, N.C.; Pop, I. Dual solutions of magnetohydrodynamic mixed convection flow of an Oldroyd-B nanofluid over a shrinking sheet with heat source/sink. *Alex. Eng. J.* **2021**, *61*, 5939–5948. [[CrossRef](#)]
24. Mabood, F.; Abbasi, A.; Farooq, W.; Hussain, Z.; Badruddin, I. Effects of non-linear radiation and chemical reaction on Oldroyd-B nanofluid near oblique stagnation point flow. *Chin. J. Phys.* **2022**, *77*, 1197–1208. [[CrossRef](#)]
25. Aziz, S.; Ahmad, I.; Ali, N.; Khan, S.U. Magnetohydrodynamic mixed convection 3-D simulations for chemically reactive couple stress nanofluid over periodically moving surface with thermal radiation. *J. Therm. Anal. Calorim.* **2020**, *146*, 435–448. [[CrossRef](#)]
26. Ahmad, I.; Aziz, S.; Khan, S.U.; Ali, N. Periodically moving surface in an Oldroyd-B fluid with variable thermal conductivity and Cattaneo-Christov heat flux features. *Heat Transf.* **2020**, *49*, 3246–3266. [[CrossRef](#)]
27. Ahmad, I.; Aziz, S.; Ali, N.; Khan, S.U. Radiative unsteady hydromagnetic 3D flow model for Jeffrey nanofluid configured by an accelerated surface with chemical reaction. *Heat Transf.* **2020**, *50*, 942–966. [[CrossRef](#)]
28. Liao, S.J. *Homotopy Analysis Method in Nonlinear Differential Equations*; Springer: Berlin/Heidelberg, Germany, 2012.
29. Al-Qudah, A.; Odibat, Z.; Shawagfeh, N. A linearization-based computational algorithm of homotopy analysis method for nonlinear reaction–diffusion systems. *Math. Comput. Simul.* **2021**, *194*, 505–522. [[CrossRef](#)]
30. Yang, Y.; Liao, S. Comparison between homotopy analysis method and homotopy renormalization method in fluid mechanics. *Eur. J. Mech.—B/Fluids* **2023**, *97*, 187–198. [[CrossRef](#)]

**Disclaimer/Publisher’s Note:** The statements, opinions and data contained in all publications are solely those of the individual author(s) and contributor(s) and not of MDPI and/or the editor(s). MDPI and/or the editor(s) disclaim responsibility for any injury to people or property resulting from any ideas, methods, instructions or products referred to in the content.